Journal of Earth Science, 2016 online *ISSN 1674-487X*
Printed in China
DOI: 10.1007/s12583-016-0924-2

Nitrate Removal by a Permeable Reactive Barrier of Fe^0: A Model-based Evaluation

Qinghua Wu[*1,2], Chunmiao Zheng[3], Jiafa Zhang[1], Fawang Zhang[4]

1. Changjiang River Scientific Research Institute, Wuhan 430010, China
2. Institute of Hydrogeology and Environmental Geology, Chinese Academy of Geological Sciences, Shijiazhuang 050061, China
3. Department of Geological Sciences, University of Alabama, Tuscaloosa, Alabama,USA
4. Institute of Karst Geology, CAGS, Guilin 541004, China

ABSTRACT: Permeable reactive barrier (PRB) filled with zero valent iron (ZVI, Fe^0) can be an effective option to remove nitrate from contaminated groundwater. The long-term performance of such PRBs, however, might be compromised by the problem of declining reactivity and permeability, which could cause a decrease in the nitrate removal efficiency. In this study we explored suitable model formulations that allow for a process-based quantification of the passivation effect on denitrification rates and tested the model for a 40 years long operation scenario. The conceptual model underlying our selected formulation assumes the declining reactivity of the ZVI material through the progressing passivation caused by the precipitation of secondary minerals and the successive depletion of the ZVI material. Two model scenarios, i.e., the base model scenario which neglects the explicit consideration of the passivation effect and one performed with the model in which the impact of the passivation effect on denitrification was considered, were compared. The modeling results illustrate that nitrate removal in the model of considered passivation started to be incomplete after 10 years, and the effluent nitrate concentration of PRB rose up to 86% of the injected water concentration after 40 years, in contrast to the base scenario, corresponding well with the field observations of successively declining nitrate removal efficiencies. The model results also showed that the porosity of the PRB increased in both models. In order to improve and recover the reactivity of ZVI, pyrite was added to the PRB, resulting in completely nitrate removal and lower consumption of ZVI.

KEY WORDS: groundwater, PRB, Zero Valent Iron, PHT3D, Denitrification

0 INTRODUCTION

Permeable reactive barriers (PRBs) have been proven to effectively remediate nitrate-contaminated groundwater (Vogan et al., 1999; Liang et al., 2005; Wilkin et al., 2002) with little or no maintenance over time (Jeen et al., 2011). Organic carbon (Schipper and Vojvodić-Vuković, 1998; Robertson et al., 2000; Robertson et al., 2007; Robertson et al., 2008) and zero valent iron (ZVI) are frequently used as the reactive material in PRBs . However, PRBs containing organic carbon can release excessive amounts of biomass into water sources, leading to secondary pollution (Rodríguez-Maroto et al., 2009). Therefore, until 2010, ZVI was used as the reactive material in more than 45% of the 150 PRBs in the United States, some of which have been successfully operating for more than 10 years (Thiruvenkatachari et al., 2008; Jeen et al., 2011). Previous studies have shown that secondary mineral precipitation in PRBs results in passivation (Jeen et al., 2007; Jin et al., 2009) and decreased porosity (Mackenzie et al., 1999; Jeen et al., 2012) over time. In one study, less iron reactivity was lost as a result of secondary mineral precipitation as the velocity of the groundwater moving through the PRB decreased during the long-term performance of a PRB (Jeen et al., 2011). In another study, the factors that affect mineral precipitation were investigated using the laboratory column method. The results indicated that $Fe(OH)_2$ was the first to precipitate, followed by $FeCO_3$ (Mackenzie et al., 1999). In addition, $CaCO_3$ only precipitated when the carbonate concentration was elevated (Mackenzie et al., 1999). Zhang and Gillham (2005) reported that the accumulation of carbonate precipitates reduced the porosity of a PRB to 7% of its initial porosity as well as the reactivity of the ZVI, according to four column tests. Furthermore, the porosity of a PRB decreases as the operation time and TDS and nitrate concentrations increase Furthermore, the porosity of a PRB decreases as the operation time and TDS and nitrate concentrations increase (Vogan et al., 1999; Kamolpornwijit et al., 2003; Liang et al., 2005).

However, a quantification method for the passivation effects of secondary mineral precipitation on the reactivity of ZVI has not yet been proposed. Moreover, since PRB porosity is affected by both secondary mineral precipitation and ZVI reactivity, the porosity increases when the rate of secondary

*Corresponding author: wqh0505@126.com

Manuscript received December 10, 2015
Manuscript accepted July 15, 2015.

Zhao, H. X., Jiang, S. Y., Dai, B. Z., et al., 2015. Geochronology and Hf Isotope Study of Pegmatite in the Xiaoqinling Area of NW China: Implication for Petrogenesis and Regional Metamorphism. *Journal of Earth Science*,doi:10.1007/s12583-016-0924-2. http://en.earth-science.net

mineral precipitation is higher than the rate of ZVI reactivity. Consequently, the mechanisms underlying the porosity changes that occur in PRBs are not well understood.

The objective of this study was to quantify the passivation effects of secondary mineral precipitation on the nitrate removal process as well as the porosity of a ZVI PRB in an idealized field scale for long-term performance using Processing Modflow 8.0 (PM). PM includes several processes that are used to manage different equations. For example, the MODEFLOW code is used to solve the water flow equation, the PHT3D code is used to solve reactive multi-component transport equations, the robust PTH3D and MT3DMS coupled code is used to solve transport equations (Zheng and Wang, 1999), and the reliable PHREEQC-2 is used to solve chemical reactions (Parkhurst and Appelo, 1999). Two models were constructed for different scenarios and compared, including model 1, in which the effects of passivation were not explicitly considered, and model 2, in which the effects of passivation on denitrification were considered. In addition, sulfur-based minerals, such as pyrite, releasing protons, can be used to dissolve precipitation on the surface of ZVI PRBs in order to enhance the nitrate removal process (Mackenzie et al., 1999). Therefore, in another model (model 3), pyrite was added to the ZVI-PRB. The effects of the added pyrite on the efficacy of the nitrate removal processes were evaluated by comparing models 1 and 3.

1 MODEL SETUP

1.1 Conceptual Model

PRBs are typically 2-50 m in length (transverse to flow), 0-5 m in width (parallel to flow), and 0-10 m in depth (RTDF, 2001). A PRB with a length of 12 m, width of 2 m, and depth of 10 m was used for the purposes of this study. The PRB, a funnel-and-gate design, was installed perpendicular to the flow of groundwater in a hypothetical site. The hypothetical site of study was 20 m in width, 80 m in length, and 13 m in depth (Fig. 1). The distance between the gate of the PRB and upper boundary was 32 m. The angle between the gate and funnel was 45°. The hydraulic conductivity of the aquifer, which was shaped like an alluvial fan, was higher in upstream regions and deep layers. Since the aquifer consisted of medium-grain sand, the hydraulic conductivity ranged from 5.8 to 8.5 (China geological survey, 2012). The funnel-shaped design of the PRB prevented the contaminated groundwater from bypassing the gate. The hydraulic conductivities of the gate and funnel of the PRB were 9 and 0.5 md^{-1}, respectively. The effective porosity values of the gate and funnel were approximately 0.5 and 0.4, respectively, resulting in an average effective aquifer porosity of approximately 0.28. Studies have shown that approximately 2.5 $molL^{-1}$-7.5×10^{-3} $molL^{-1}$ of nitrate is effectively removed by PRBs (Robertson and Cherry, 1995; Robertson et.al, 2000; Robertson et.al, 2008). Therefore, a nitrate concentration of 5.0×10^{-3} $molL^{-1}$ was selected for the contaminated groundwater. The groundwater was continually injected into the aquifer at a rate of 10 m^3d^{-1}. The injected well was installed in the middle of the gate and upper boundary.

The PRB consisted of iron filling with a 40-grain mesh and density of 3.0gcm^{-3} (15%), coarse sand (35%), and water (50%) (Robertson et al., 2000). The surface area of the ZVI was approximately 0.11m^2g^{-1} (Cohen et al., 2009). After the addition of the pyrite, only 9.58% of the sand in the PRB was replaced by 4$molL^{-1}$bulk pyrite.

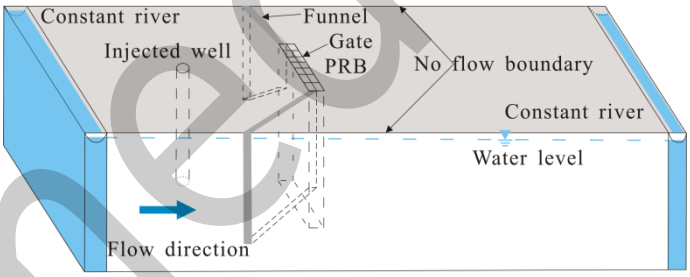

Figure 1. Schematic of a ZVI-based PRB used to remove nitrate from groundwater. The distance between the injected well and PRB was 15.0 m.

1.2 Flow and Transport Model

The model (80 m × 20 m × 13 m) was divided into 6 vertical layers. The first layer, which was considered to be an unconfined aquifer, was 3.0 m in depth, while the remaining layers were 2.0 m in depth. The model, excluding the PRB zone (0.4 m × 1 m) was further discretized into horizontal grid cells (2 m × 2 m). A time step of 1 day was used for the purposes of this study. The heads in both the inflow and outflow boundaries of the model remained constant at 12.5 m and 12.0 m, respectively. In addition, left and right boundaries were no-flow boundaries. The longitudinal dispersivity of all of the cells in the model was 0.5 m. The solution scheme of flow and transport modeling are finite-difference and the iterative PCG2 (Preconditioned Conjugate-Gradient 2) and GCG (Generalized Conjugate Gradient) solver are used, respectively.

1.3 Geochemical Reaction Model

The MT3DMS code was used to model solute transport in the PM, while the PHREEQC-2 code was used to model the geochemical reactions. All of the aqueous and phase species were calculated and simulated by applying either equilibrium or kinetic reactions with strict mole and charge-balance requirements to the complicated, multi-component system. In this study, the dissolution of the ZVI was assumed to occur via equilibrium reactions, in which donated electrons were gradually consumed by electron acceptors in the kinetic reactions (Table 1). The end product of the ZVI-facilitated denitrification was either nitrogen (Till et al., 1998; Choe et al., 2000) or am-

monium (Alowitz and Scherer, 2002; Zhang et al., 2010), with an intermediate product of nitrite. In addition, nitrogen was assumed to be the product of dentrification .

Table1 Reduction-corrosion reactions

Reactant	Reaction
ZVI	$Fe^0 \rightarrow Fe^{2+} + 2e^-$
Oxygen	$O_2 + 4H^+ + 4e^- \rightarrow 2H_2O$
Nitrate	$2NO_3^- + 12H^+ + 10e^- \rightarrow N_2 + 6H_2O$
Ferric iron	$Fe^{3+} + e^- \rightarrow Fe^{2+}$
Sulfate	$SO_4^{2-} + 9H^+ + 8e^- \rightarrow HS^- + 4H_2O$
Carbonate	$CO_3^{2-} + 10H^+ + 8e^- \rightarrow CH_4 + 3H_2O$
Water	$Fe^0 + 2H_2O \rightarrow Fe^{2+} + 2OH^- + H_2$

Previous studies have shown that the rate constants of ZVI-corrosion reaction were proportional to the surface of ZVI (Huang and Zhang, 2002; Zhang et al., 2010). Secondary mineral precipitation and ZVI dissolution result in decreased ZVI surface area per bulk PRB volume. Therefore, the ZVI surface area should be updated to kinetic rates in order to simulate the effects of reduced ZVI surface area on iron corrosion. The reactive surface area of ZVI can be expressed with an empirical relationship that accounts for the effects of secondary mineral precipitation and ZVI deterioration as (Jeen et al., 2007):

$$S(t) = S_0 \cdot \exp\left(-\sum_i a_i \varphi_i(t)\right) \cdot \left(\frac{\varphi_{Fe^0}}{\varphi^0_{Fe^0}}\right)^{2/3} \quad (1)$$

$$S(t) = S_0 \cdot \exp\left(-\sum_i a_i \varphi_i(t)\right) \cdot \left(\frac{C_{Fe^0}}{C^0_{Fe^0}}\right)^{2/3} \quad (2)$$

where S(t) and S_0 represent the reactive surface area of a ZVI at times t and t=0 (m^2 iron L^{-1} bulk), respectively; a_i is an empirical proportionality constant that describes the relationship between ZVI reactivity loss and the secondary mineral precipitation phase i; $\varphi_i(t)$ represents the volume fraction of the secondary mineral phase i(-); φ_{Fe^0} and $\varphi^0_{Fe^0}$ represent the volume of the ZVI(-) at times t and t=0, respectively; and C_{Fe^0} and $C^0_{Fe^0}$ represent the concentrations of the ZVI ($molL^{-1}$ bulk of PRB) at times t and t=0, respectively. Secondary mineral precipitation can be expressed as

$$r_i^m = -k_{eff,i}\left(1 - \frac{IAP_i^m}{K_i^m}\right)^{H_2O} \quad (3)$$

where $k_{eff,i}$ is a constant that represents the rate of the secondary mineral phase i ($molL^{-1}$ day^{-1}), IAP_i^m is the ion activity product of phase i (calculated as the equilibrium constant of both the equilibrium and non-equilibrium states), and K_i^m is the equilibrium constant of phase i.

Most studies have demonstrated that reaction rates can be expressed by first-order kinetic equations (Zhang et al., 2010; Hwang et al., 2011) or pseudo-first-order equations (Zhang et al., 2010). In this study, the rates of the reduction-corrosion reactions were expressed as Monod kinetic equations in order to account for the electron acceptors, including oxygen, nitrate, sulfate, ferric iron, carbonate, and even water (Prommer et al., 2008; Cohen et al., 2009). Therefore, ZVI deterioration can be expressed by the sum of progressive electron consumption by electron acceptors as

$$-\frac{dC_{Fe^0}}{dt} = r_{O_2} + r_{NO_3^-} + r_{Fe^{3+}} + r_{SO_4^{2-}} + r_{CO_3^{2-}} + r_{H_2O} \quad (4)$$

where r_{O_2}, $r_{NO_3^-}$, $r_{Fe^{3+}}$, $r_{SO_4^{2-}}$, $r_{CO_3^{2-}}$, and r_{H_2O} represent the contributions from reduction-corrosion of oxygen, nitrate, ferric iron, sulfate, carbonate, and water, respectively. Each of the corrosion reactions was described in the Monod kinetic equation. However, the presence of oxygen in the reaction system inhibits the degradation facilitated by other electron acceptors. Therefore, a term was added to the Monod kinetic reaction in order to account for any reductions in the reaction rate resulting from the presence of electron acceptors with higher oxidation capabilities (Clement, 1997):

$$r_{O_2} = -k_{eff,O_2}\frac{C_{O_2}}{K_{O_2}+C_{O_2}} \quad (5)$$

$$r_{NO_3^-} = -k_{eff,NO_3^-}\frac{C_{NO_3^-}}{K_{NO_3^-}+C_{NO_3^-}}\frac{K_{inh,O_2}}{K_{inh,O_2}+C_{O_2}} \quad (6)$$

$$r_{Fe^{3+}} = -k_{eff,Fe^{3+}}\frac{C_{Fe^{3+}}}{K_{Fe^{3+}}+C_{Fe^{3+}}}\frac{K_{inh,O_2}}{K_{inh,O_2}+C_{O_2}}\frac{K_{inh,NO_3^-}}{K_{inh,NO_3^-}+C_{NO_3^-}} \quad (7)$$

$$r_{SO_4^{2-}} = -k_{eff,SO_4^{2-}}\frac{C_{SO_4^{2-}}}{K_{SO_4^{2-}}+C_{Fe^{3+}}}\frac{K_{inh,O_2}}{K_{inh,O_2}+C_{O_2}}\frac{K_{inh,NO_3^-}}{K_{inh,NO_3^-}+C_{NO_3^-}}\frac{K_{inh,Fe^{3+}}}{K_{inh,Fe^{3+}}+C_{Fe^{3+}}} \quad (8)$$

$$r_{CO_3^{2-}} = -k_{eff,CO_3^{2-}}\frac{C_{CO_3^{2-}}}{K_{CO_3^{2-}}+C_{CO_3^{2-}}}\frac{K_{inh,O_2}}{K_{inh,O_2}+C_{O_2}}\frac{K_{inh,NO_3^-}}{K_{inh,NO_3^-}+C_{NO_3^-}}\frac{K_{inh,Fe^{3+}}}{K_{inh,Fe^{3+}}+C_{Fe^{3+}}}\frac{K_{inh,SO_4^{2-}}}{K_{inh,SO_4^{2-}}+C_{SO_4^{2-}}} \quad (9)$$

i where C_{O_2}, $C_{NO_3^-}$, $C_{Fe^{3+}}$, $C_{SO_4^{2-}}$, and $C_{CO_3^{2-}}$ represent the concentrations of oxygen, nitrate, ferric iron, sulfate, and carbonate ($molL^{-1}$), respectively; k_{eff,O_2}, k_{eff,NO_3^-}, $k_{eff,Fe^{3+}}$, $k_{eff,SO_4^{2-}}$, and $k_{eff,CO_3^{2-}}$ represent the constant reaction rates of the electron acceptors ($molL^{-1}day^{-1}$); K_{O_2}, $K_{NO_3^-}$, $K_{Fe^{3+}}$, $K_{SO_4^{2-}}$, and $K_{CO_3^{2-}}$ represent the half-saturation constants of the electron acceptors ($molL^{-1}$); and K_{inh,O_2}, K_{inh,NO_3^-}, $K_{inh,Fe^{3+}}$, and $K_{inh,SO_4^{2-}}$ represent the inhibition constants of the oxygen, nitrate, ferric iron,

and sulfate (molL^{-1}), respectively. The rates of water-iron corrosion and secondary mineral precipitation can be expressed using a first-order equation as

$$r_{H_2O} = -\max\left\{k_{eff H_2O}\left(1-\frac{IAP(Fe^{2+})}{K_{H_2O-Fe^0}}\right), 0\right\} \quad (10)$$

where $k_{eff H_2O}$ represents the constant rate of iron corrosion (molL^{-1}day^{-1}), $IAP(Fe^{2+})$ represents the iron activity product, and $K_{H_2O-Fe^0}$ represents the equilibrium constant. The kinetic rate expression for the iron corrosion in the model was updated by formula (1), which was related to the surface area of ZVI per bulk volume. Therefore, the updated kinetic rate of iron corrosion is expressed as

$$-\frac{dC_{Fe^0}}{dt} = (r_{O_2} + r_{NO_3^-} + r_{Fe^{3+}} + r_{SO_4^{2-}} + r_{CO_3^{2-}} + r_{H_2O}) * \frac{S(t)}{S_0} \quad (11)$$

1.4 Model Parameters

The secondary minerals that precipitate in PRBs over time primarily include Calcite ($CaCO_3$), $Fe(OH)_3$(am), $Fe(OH)_2$(am), and FeS (Mackenzie et al., 1999; Johnson et al., 2008; Jeen et al., 2012). The rate constants of the kinetic reactions used to describe reduction-corrosion and secondary mineral precipitation are shown in Table 2. The proportionality constants of calcite, $Fe(OH)_3$(am), $Fe(OH)_2$(am), and FeS are approximately 90 (Jin et al., 2009), 2, 2 (Jeen et al., 2007), and 1, respectively. The other reactions parameters, such as the equilibrium parameters of the secondary minerals, were obtained from the PHREEQC-2 database.

In order to simulate the effects of the inhibition of secondary mineral precipitation on ZVI reactivity and the nitrate removal process, the contaminated groundwater, which contained Ca^{2+}, CO_3^{2-} and NO_3^-, Cl^-, and O_2, was injected upstream from the PRB. The concentrations of the aqueous species in the background water and injection well of the model are listed in Table 3.

Table 2 Secondary mineral precipitation and redox reaction parameters

Oxidant				Secondary mineral		
	$logk_{eff}$ (molL^{-1}s^{-1})	$logK_{oxidant}$ (molL^{-1})	$logK_{inh,oxidant}$ (molL^{-1})		$logk_{eff}$ (molL^{-1}s^{-1})	$logK_i^m$
Oxygen	-6.0	-4.0 [b]	-7.50 [c]	Calcite($CaCO_3$)	-8.80	-8.48 [d]
Nitrate	-6.52 [a]	-4.0 [b]	-7.80 [c]	$Fe(OH)_3$(am)	-14.0	4.891 [d]
Ferric iron	-7.07 [a]	-4.0 [b]	-7.75 [c]	$Fe(OH)_2$(am)	-14.0	13.56 [d]
Sulfate	-8.0 [a]	-4.0 [b]	-7.98 [c]	FeS(ppt)	-14.0	-3.92 [d]
Carbonate	-11.0	-4.0 [b]				
Water	-9.30 [a]					

a) Obtained from Mayer et al., 2001; b) Obtained from Prommer et al., 2008; c) Obtained from Clement, 1997; d) Obtained from Parkhurst and Appelo, 1999. Other data was supposed for modeling according to previous papers.

Table 3 Chemical compositions of the background and contaminated water (molL^{-1})

background water				contaminated water			
species	concentration	species	concentration	species	concentration	species	concentration
Na^+	1.0×10^{-4}	Cl^-	3.4×10^{-4}	Na^+	1.0×10^{-4}	CO_3^{2-}	3.0×10^{-3}
K^+	2.0×10^{-3}	CO_3^{2-}	1.0×10^{-3}	K^+	2.0×10^{-3}	N(+5)	5.0×10^{-3}
Ca^{2+}	1.0×10^{-3}	O(0)	6.25×10^{-3}	Ca^{2+}	5.0×10^{-3}	Cl^-	1.032×10^{-3}
Mg^{2+}	1.0×10^{-3}	pH	7.0	Mg^{2+}	1.0×10^{-3}	O(0)	1.56×10^{-4}
Fe(+3)	2.0×10^{-3}	pe	13.5	Fe(+3)	2.0×10^{-3}	pH	7.0
S(6)	4.0×10^{-3}			S(6)	4.0×10^{-3}	pe	13.5

* Cl^- charge-balanced specie in the models

2 RESULTS and DISCUSSION

2.1 Tracer Test

In order to investigate the nitrate-removal efficiency of the PRB, a compared tracer test was conducted using 5.0×10^{-3} molL^{-1} NaBr (equal to the nitrate concentration) (Fig. 2). The results indicated that the contaminated water with nitrate was captured successfully by the PRB and primarily flowed through the ZVI reactive zone (Fig. 2a). The average pore velocity of the groundwater was approximately 0.33md-1, with a residence time of 6 days in the PRB.

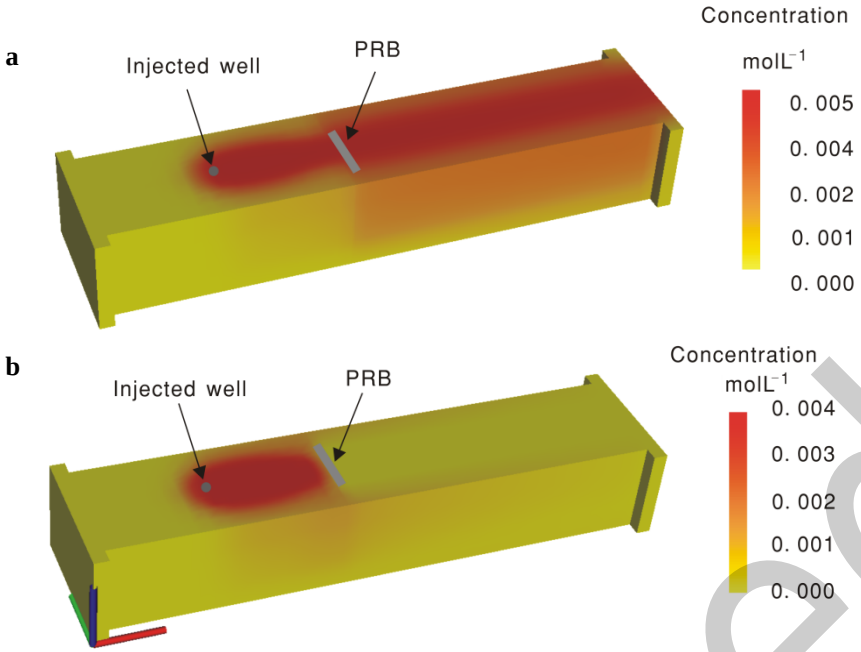

Figure 2 Solute plumes 365 days after source injection: a) conservative tracer; b) amount of nitrate removed by the ZVI after crossing the PRB model with the updated rate

2.2 Nitrate Removal

5.1 Crystallization Age of the Pegmatite Dyke

The electron acceptors that facilitated iron corrosion included oxygen, nitrate, ferric iron, sulfate, and carbonate, in that sequence. The latter (e.g., nitrate) was inhibited by the former (e.g., oxygen) in the presence of multi- electron acceptors (Clement, 1997), supposing that the water-corrosion reaction was not affected by the other electron acceptors (Prommer et al., 2008; Cohen et al., 2009). In order to evaluate the effects of the reduction in ZVI reactivity resulting from secondary mineral precipitation and mass loss of ZVI on the removal of nitrate, simulations were conducted using models with and without the updated iron reactivity rate, or models 1 and 2, respectively. The results obtained using both models are shown in Figs. 3-5.

In model 1, nitrate first appeared in the upstream boundary of the reactive zone in the third layer of the PRB model after 1300 days, indicating that the rate of nitrate removal decreased as both time and the distance to the entrance of the PRB increased as a result of the reduction in the denitrification rate. Before 3800 days of operation, the nitrate was removed completely by the PRB, resulting in a constant nitrogen concentration (the end product of denitrification). However, after 3800 days of operation, the nitrate broke though the PRB, meaning the PRB no longer had the ability to clean up the nitrate completely, and the concentration of nitrate increased gradually to 4.29×10^{-3} molL^{-1} (86% of the injected concentration), while the nitrogen concentration decreased (Figs. 2b and 3a) (Jin et al., 2009; Jeen et al., 2011). Due to the passivation of secondary minerals and mass ZVI loss, the nitrate removal efficiency decreased over time. In fact, only 15% of the nitrate concentration was removed from the contaminated water over 40 years of operations (Figs. 3a and 4a). The constant rates of denitrification could increase if smaller iron particles with a larger surface area of ZVI were selected. However, the higher rate of denitrification would produce too much gas (e.g., hydrogen and nitrogen) to escape from the PRB, causing the flow clogging problem and shorter system lifetime (Jeen et al. 2012). Moreover, particle-to-particle contact would occur more frequently if smaller iron particles were used, resulting in decreased hydraulic conductivity. However, neglecting secondary mineral passivation, the denitrification rates in the laboratory were several of orders of magnitude larger than those in the model. For example, the denitrification rate of a nanoscale ZVI with a surface area of 12.4m^{2}g^{-1} was 20 times higher than that of 0.49 m^{2}g^{-1} of Fe^0 powder (Zhang et al., 2010). Therefore, the results of the laboratory experiments could not be directly applied to long-term modeling, especially in the presence of calcite fouling.

In model 2, the nitrate was removed completely, and the nitrogen concentration remained constant at 4.6×10^{-3} molL^{-1} over 40 years of operation (Fig. 3a). These results have not been observed in previous field studies concerning the long-term operation of PRBs (Jeen et al., 2006; Henderson and Demond, 2007; Johnson et al., 2008).

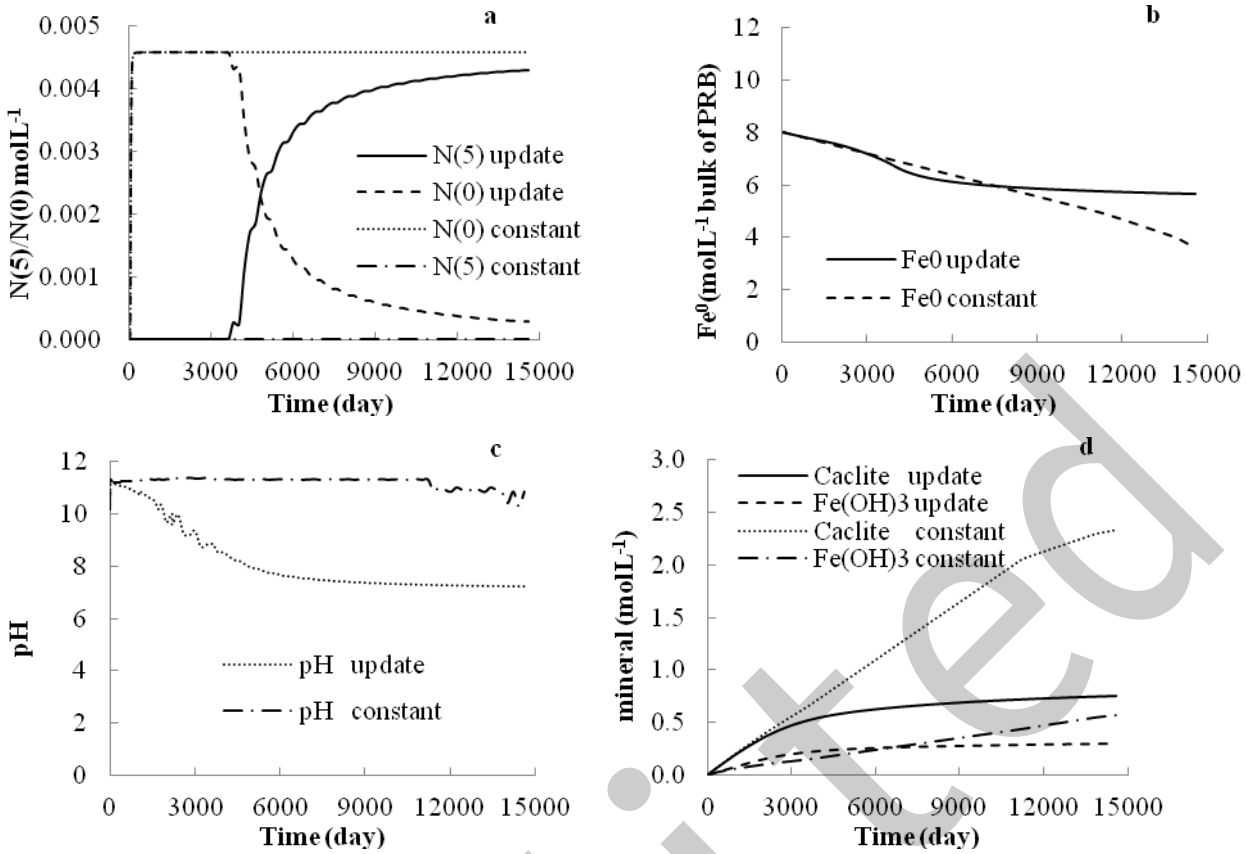

Figure 3 Simulation results obtained using both models at the effluent face of the PRB (entrance face for secondary minerals) in the third layer over an operation time of 40 years: (a) nitrate and nitrogen, (b) ZVI, (c) pH, and (d) secondary minerals

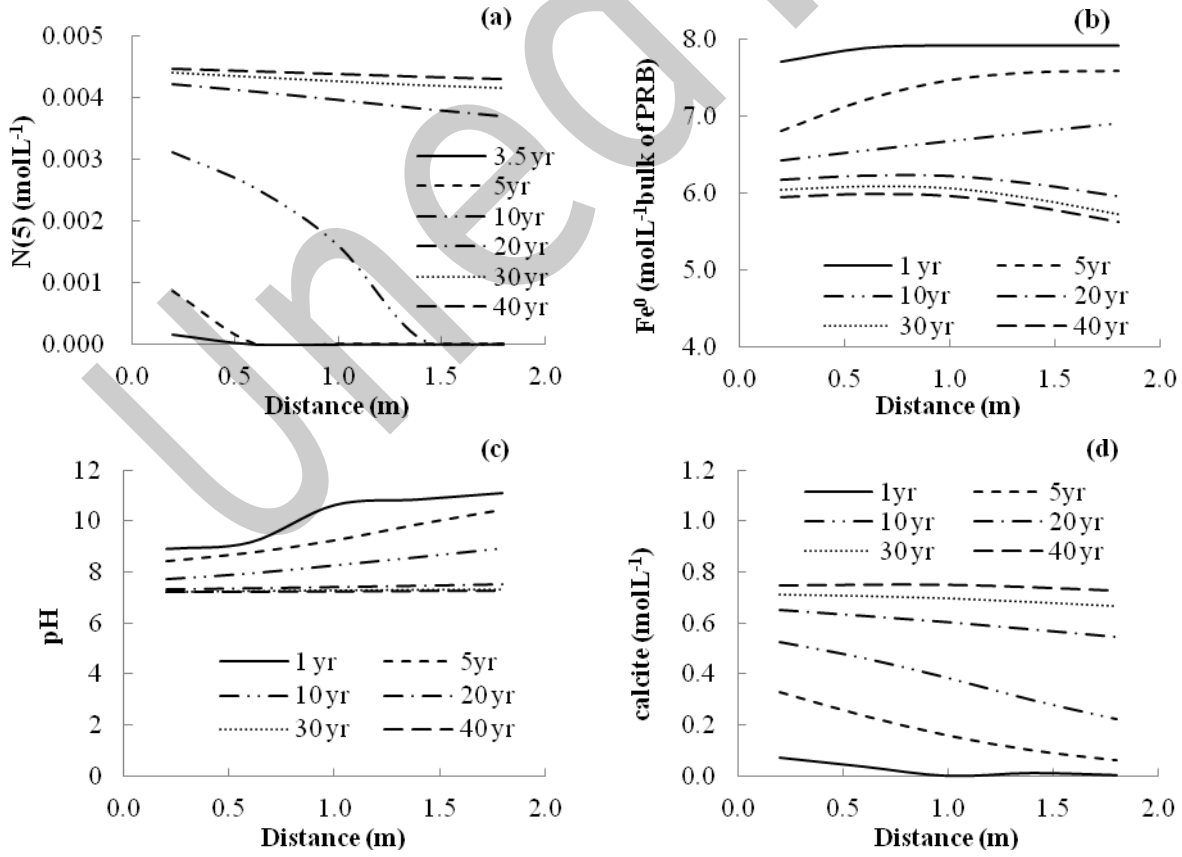

Figure 4 Simulation results obtained using model 1. Readings were obtained along the flow path in the third layer of the ZVI after 1, 5, 10, 20, 30, and 40 years of operation: (a) nitrate, (b) ZVI, (c) pH, and (d) calcite

2.3 ZVI Reactivity

According to formulas (1) and (11), the decreased reactivity of ZVIs primarily results from the decreased surface area of ZVIs per bulk volume and the passivation of secondary mineral precipitation. Column studies have shown that the denitrification rate increases as the ZVI dose increases, primarily due to the increased surface area of Fe^0 per bulk volume (Choe et al., 2000; Rodríguez-Maroto et al., 2009; Zhang et al., 2010). In addition, the long-term performance of PRBs has been proven to be influenced by the secondary precipitation of minerals, primarily calcite, due to the passivation of iron and resulting decrease in reaction rate (Zhangl and Gillham, 2005; Jeen et al., 2006).

As the reactivity of the ZVI decreased, the rate of iron corrosion decreased gradually, resulting in less ZVI deterioration. In addition, in model 1, the remaining ZVI concentration from 3800 to 7600 days was lower than that in model 2 (Fig. 3b). The possible reason was that Fe^{2+} in model 1 was oxidized to Fe^{3+} by the nitrate content, accelerating the precipitation of $Fe(OH)_3$ (am), with small proportionality constant of 2 (Jeen et al., 2007; Jin et al., 2009) in model 1 reducing the concentration of Fe^{2+} and increasing the dissolution of ZVI.

The average percentage of ZVI dissolution that occurred over 40 years in the downstream regions of the two PRB models were approximately 30% and 55%, respectively. In model 1, the ZVI concentration was highest along the direction of water flow during the first 14 years of operation; however, the inverse was true after 14 years of operation (Fig. 4b). This was attributed to the initial removal of nitrate as it flowed into the entrance of the PRB. However, the accumulation of calcite precipitates on the surface of the ZVI increased iron passivation after long-term operation, resulting in the removal of the majority of the nitrate and oxidants in the downstream region of the PRB. Without considering the secondary mineral precipitation in model 2, most of oxygen and nitrate were initially reduced and removed at the entrance of PRB where the ZVI was consumed completely in 30.7 years, causing the high amount of remnant ZVI along the flow path until the ZVI was depleted (Fig. 5a).

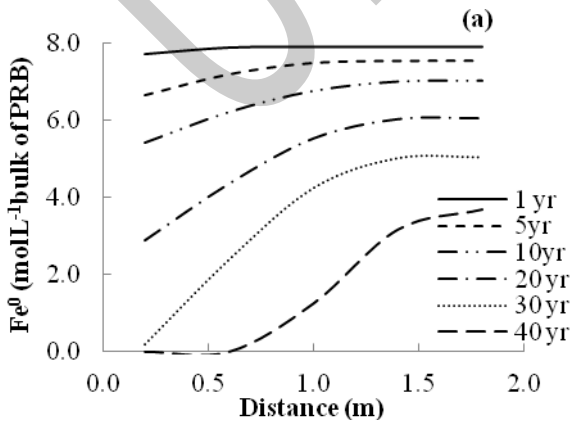

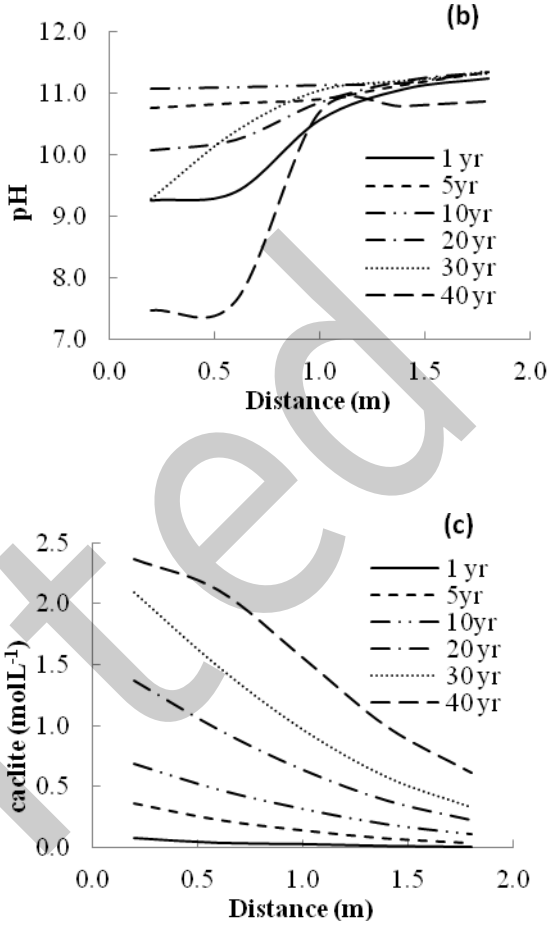

Figure 5 Simulation results obtained using model 2. Readings were obtained along the flow path in the third layer of the ZVI after 2, 5, 10, 20, 30, and 40 years of operation: (a) ZVI, (b) pH, and (c) calcite. Nitrate concentrations are not shown since the nitrate was removed by the PRB.

2.4 pH

Previous studies have shown that pH significantly affects denitrification in ZVI reactive systems. In fact, the rate of nitrate removal at a pH of less than 5 has been proven to significantly higher than at a pH of greater than 6. In addition, pH and the pseudo-first rate constant exhibit a positive, linear relationship at unregulated pH values of 7.0-11.0 in the absence of secondary mineral precipitation (Choe et al., 2004; Chen et al., 2005).

In both models, the oxygen and sulfate were initially reduced by the ZVI, resulting in a significant increase in pH from 7.0 to 10.1 in 1 day. Once the oxygen content had been depleted, the nitrate content from the injected wells was removed, resulting in a gradual increase in pH to 11.0 in the first 20 days and 11.4 within 50 days (Fig. 3c). These results have also been observed in experimental studies, in which the pH increased significantly within as few as 2 hours (Huang and Zhang, 2002; Choe et al., 2004; Hwang et al., 2011). However, after 50 days,

the pH decreased gradually in the downstream region of the PRB in model 1 due to the precipitation of $Fe(OH)_3$ (am) and dilution of the injected and background water. However, these changes were not observed in model 2 (Fig. 3c). As shown in Figs. 4c and 5b, the pH increased along the flow of water over time.

2.5 Secondary Mineral Precipitation

The precipitation of secondary minerals resulted in the passivation of iron over time and, thereby, reduced ZVI reactivity. The precipitation of calcite and $Fe(OH)_3$ (am) was controlled by the pH and corrosion of iron within the reactive system (Fig. 3c). The high pH accelerated the precipitation of secondary minerals (Johnson et al., 2008; Thiruvenkatachari et al., 2008). Due to the accumulation of secondary mineral precipitates, especially calcite, in model 1, iron passivation at the entrance of the PRB increased over time. As a result, model 1 exhibited lower pH values and less precipitation than model 2, in which the rate of calcite precipitation remained constant over time. According to the simulation results obtained using the two models, the calcite concentrations decreased along the flow of water. In addition, the calcite concentration was much higher in model 1 than in model 2, with concentrations of 2.37 and 0.75 $molL^{-1}$ at the entrance of the PRB after 40 years of operation, respectively. The $Fe(OH)_2$ and FeS contents are not discussed herein since their concentrations were relatively low.

2.6 Porosity

The precipitation of secondary minerals decreased the porosity of the PRB, while the dissolution of the ZVI increased the porosity of the PRB (Fig. 6). Most of the changes in porosity occurred at the entrance of the PRB, where most of the secondary minerals precipitated (Li et al., 2005; Jin et al., 2009; Jeen et al., 2012). However, the simulation results indicated that the total porosity of the PRBs in models 1 and 2 increased by 0.0011 and 0.043 after 40 years of operation, respectively. These results conflicted with the results of previous studies (Fig 6b). This was attributed to the relatively high rate of ZVI dissolution in the models herein; the relatively high concentrations of oxidants, such as oxygen ($1.56\times10^{-4}molL^{-1}$), nitrate ($5\times10^{-3}molL^{-1}$), and ferric iron ($2\times10^{-5}molL^{-1}$), which significantly increased the porosity of the PRBs (Fig. 6a). In addition, relatively low constant $Fe(OH)_3$ (am), $Fe(OH)_2$, and FeS rates were used in order to make the PHT3D converge easily and cost much less time to model for 40 years of operation. Furthermore, the velocity of the groundwater moving through the PRB was high ($0.33md^{-1}$), resulting in less resident time within the PRB and decreased secondary mineral precipitation (Fig. 6a). Therefore, the ZVI without the updated rate became depleted after only 30 years of operation, resulting in an increased porosity of 0.15 (i.e., the initial percentage of the ZVI in the PRB). However, the secondary mineral precipitation decreased the porosity by 0.09. Thus, although the reduction in hydraulic conductivity prevented the movement of contaminated water through the PRB over time, especially in model 2, which exhibited a much higher rate of ZVI dissolution than model 1, it was not necessary to consider the effect of hydraulic conductivity change on nitrate removal by the PRB. (Fig. 6b).

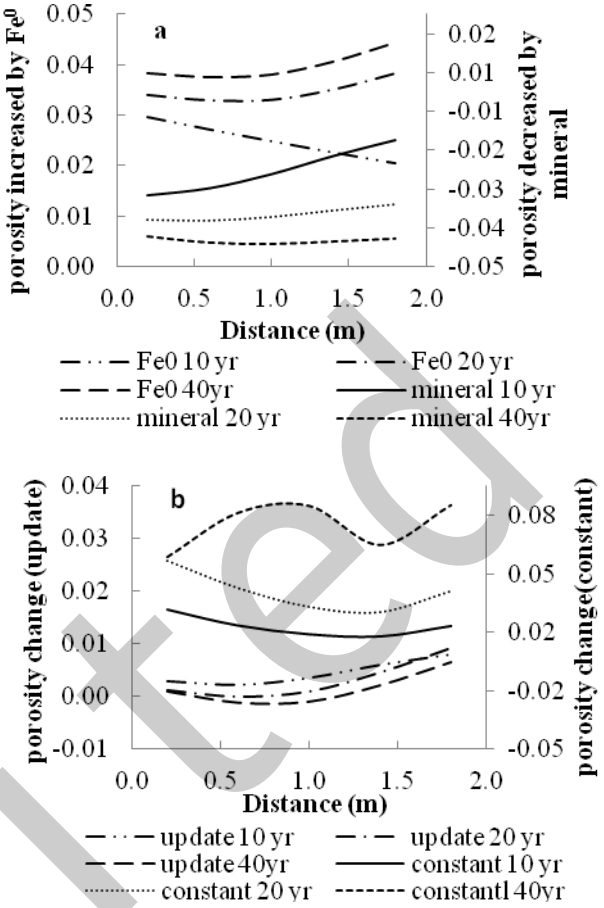

Figure 6 Change in porosity over time. Readings were obtained along the flow path after 10, 20, and 40 years of operation. Positive data was used to represent increased PRB porosity, while negative data was used to represent decreased PRB porosity. (a) In model 1, the porosity increased by Fe0 and decreased by minerals. (b) Total change in porosity in both models.

2.7 Effects of Buffering Minerals

The iron corrosion reactions significantly increased the pH, resulting in a significant reduction in the rate of denitrification (Choe et al., 2004; Liou et al., 2005). This resulted in the movement of nitrate through the PRB and, thereby, low nitrate removal efficiency (Fig. 2b, 3a, 4a). Therefore, 9.58% ($4molL^{-1}$bulk of the PRB) of pyrite (FeS_2) was added to the PRB as a buffering mineral to control the pH of the reactive system (Mackenzie et al., 1999). The pyrite also acted as an electron donor for Fe^0 during a certain period of time (-log[e] in water, where e denotes an electron). The other parameters of this model (model 3) were equal to those of model 1. Initially, small amounts of pyrite were produced and began to dissolve after 30 days of operation as the water-enriched nitrate (5×10^{-3} $molL^{-1}$) and oxygen (1.56×10^{-4} $molL^{-1}$) reached the entrance of the PRB. The pyrite was then oxidized to sulfate and released protons required for iron corrosion, resulting in a relatively high concentration of sulfate (3.3×10^{-3} $molL^{-1}$) compared to model 1 (4.0×10^{-5} $molL^{-1}$, equal to that of the background and injected water). Within the 40 years of operation, all of the nitrate

and 50% of the pyrite was removed, with only 6% ZVI dissolution (Fig 7a). These results indicated that the introduction of more pyrite and less ZVI could increase the lifetime of PRBs while lowering associated costs. However, compared to model 1, the pH did not decrease as significantly within the first 10 years of operation (Fig. 7b). According to the results obtained using model 1, iron passivation resulting from the accumulation of secondary mineral precipitates resulted in decreased nitrate removal rates and the movement of nitrate through the PRB after 3800 days of operation. The pH then gradually decreased over time due to the flushing of background water, which had a pH of 7.0, and a reduction in the availability of hydroxyl ions. Therefore, the pH in model 3 was higher than that in model 1 after long-term operation (Fig 7.b). As shown in Fig. 7c, the total porosity decreased in model 3. In contrast, the total porosity increased in models 1 and 2. The porosity of the PRB along the flow of water varied over time due to decreased FeS_2 and ZVI dissolution and the equivalent precipitation of secondary minerals.

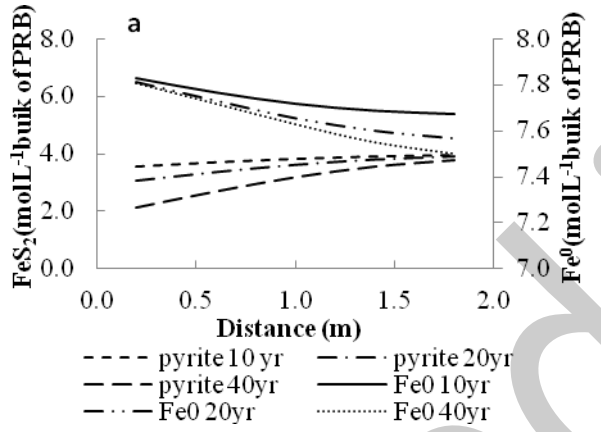

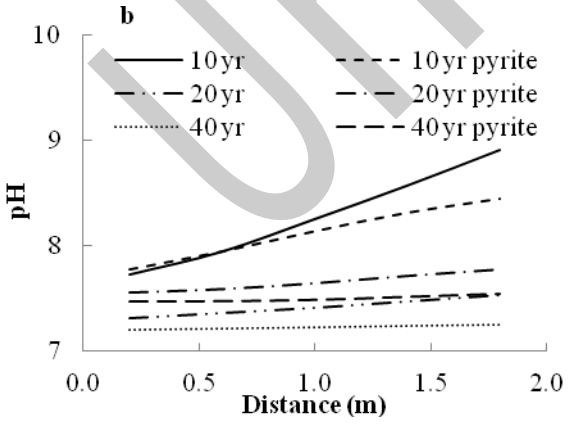

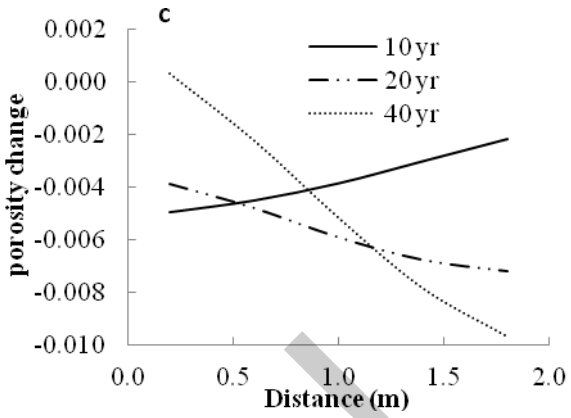

Figure 7 Simulation results obtained using the models with the updated rate after the addition of pyrite. Readings were obtained along the flow path of the PRB after 10, 20, and 40 years of operation: (a) relationship between the dissolution of pyrite and the ZVI, (b) comparison of the pH values obtained using models 2 and 3, and (c) total change in porosity. Positive data was used to represent increased PRB porosity, while negative data was used to represent decreased PRB porosity.

3 CONCLUSIONS

In this paper, the denitrification in a ZVI-based PRB over time was simulated using a PTH3D model based on the effects of secondary mineral precipitation, considering the inhibitory effects of secondary mineral precipitation and ZVI dissolution on iron corrosion. A series of simulations were conducted in order to evaluate various scenarios. The results indicated that the model with the rate update predicted PRB denitrification more effectively than the model without the rate update. As the reactivity of the ZVI decreased, the nitrate passed through the PRB after the first few years of operation. However, according to the results obtained by the model without the rate update, the nitrate was completely removed from the contaminated water within the operation period. These effects have not been observed in previous field studies. As the nitrate, oxygen, and ferric iron were removed from the contaminated water, the total porosity of the PRB increased rather than decreased as demonstrated in previous studies. This resulted in an increased iron corrosion rate and decreased constant rates of secondary mineral fouling. In order to resolve the decreased nitrate removal efficiency that had occurred after approximately 10 years of operation, pyrite was added to the PRB. The addition of pyrite resulted in the complete removal of nitrate and decreased ZVI dissolution. Although the model developed in this paper could be used to facilitate nitrate removal during long-term PRB operation, all of the parameters used in this study were obtained from laboratories and previous long-term field studies. In addition, increased iron corrosion and secondary mineral precipitation rates could prevent the PHT3D code from converging efficiently and increase computation times. The hydraulic conductivity must be updated to a kinetic rate in long-term modeling when the iron corrosion rate is low and Ca^{2+} and CO_3^{2-} concentrations are high.

ACKNOWLEDGEMENTS

The authors are grateful for advices for the model setup by

Rui Ma and Guoliang Cao. The study was supported by a scholarship from the National Natural Science Foundation of China (41402213 and 51279016) , Open Fund of Three Gorges Research Center for Geo-hazard, Ministry of Education, China University of Geosciences (TGRC201403), Open Fund of Institute of Hydrogeology and Environmental Geology, CAGS (KF201508), and Technology Foundation for Selected Overseas Chinese Scholar, Ministry of Personnel of China (2014).

REFERENCES CITED

Alowitz, M. J., Scherer, M. M., 2002. Kinetics of Nitrate, Nitrite, and Cr (VI) Reduction by Iron Metal. *Environmental Science & Technology* , 36(3): 299-306.

Chen, Y., Li, C., Chen, S., 2005. Fluidized Zero Valent Iron Bed Reactor for Nitrate Removal. *Chemosphere*, 59(6):753-759.

China Geological Survey. 2012. Handbook of Hydrogeology (second version). Geological Publishing House.

Choe, S., Chang, Y., Hwang, K., et al., 2000. Kinetics of Reductive Denitrification by Nanoscale Zero-valent Iron. *Chemosphere*, 41(8): 1307-1311.

Choe, S., Liljestrand, H. M., Khim, J., 2004. Nitrate Reduction by Zero-Valent Iron under Different pH Regimes. *Applied Geochemistry*, 19(3): 335-342.

Clement, T. P., 1997. RT3D: A Modular Computer Code for Simulating Reactive Multi-species Transport in 3-Dimensional Groundwater Aquifers. PNNL-SA-11720. Richland, Washington: Pacific Northwest National Laboratory.

Cohen, E. L., Patterson, B. M., Mckinley, A.J., et al., 2009. Zero Valent Iron Remediation of A Mixed Brominated Ethene Contaminated Groundwater. *Journal of Contaminant Hydrology*, 103(3-4):109-118.

Liou, Y. H., LO, S. L., Lin, C. J., et al., 2005. Methods for Accelerating Nitrate Reduction Using Zero Valentiron at Near-Neutral pH : Effects of H_2-Reducing Pretreatment and Copper Deposition. *Environmental Science & Technology*, 39(24):9643-9648.

Henderson, A. D., Demond, A. H., 2007. Long-term Performance of Zero-Valent Iron Permeable Reactive Barriers: A Critical Review. *ENVIRONMENTAL ENGINEERING SCIENCE*, 24(4):401-423.

Huang, Y.H., Zhang, T.C., 2002. Kinetics of Nitrate Reduction by Iron at Near Neutral pH. *Journal of Environmental Engineering*.128(7): 604-611.

Hwang, Y., Kim, D., Shin, H., 2011. Mechanism Study of Nitrate Reduction by Nano Zero Valent Iron. *Journal of Hazardous Materials*, 185(2-3): 1513-1521.

Jeen, S., Amos, R.T., Blowes, D.W., 2012. Modeling Gas Formation and Mineral Precipitation in a Granular Iron column. *Environmental Science & Technology*, 46(12): 6742-6749.

Jeen, S., Gillham, R.W., and Przepiora, A., 2011. Predictions of Long-term Performance of Granular iron Permeable Reactive Barriers : Field-scale Evaluation. *Journal of Contaminant Hydrology*, *123*(1-2):50-64.

Jeen, S., Gillham, R. W., Blowes, D.W., 2006. Effects of Carbonate Precipitates on Long-term Performance of Granular Iron for Reductive Dechlorination of TCE. *Environmental Science & Technology*, 40(20): 6432-6437.

Jeen, S., Mayer, K.U., Gillham, R.W., et al., 2007. Reactive Transport Modeling of Trichloroethene Treatment with Declining Reactivity of Iron. *Environmental Science & Technology*, 41(4):1432-1438.

Jin, S. O., Jeen, S., Gillham, R., Gui, L., 2009. Effects of Initial Iron Corrosion Rate on Long-term Performance of Iron Permeable Reactive Barriers : Column Experiments and Numerical Simulation. *Journal of Contaminant Hydrology*, 103(3-4):145-156.

Johnson, R. L., Thoms, R. B., Johnson, R.O., et al., 2008. Mineral Precipitation Upgradient from A zero-valent Iron Permeable Reactive Barrier. *Ground Water Monitoring and Remediation*, 28 (3), 56-64.

Kamolpornwijit, W., Liang, L., West, O.R., et al., 2003. Preferential Flow Path Development and Its Influence on Long-term PRB Performance: Column Study. *Journal of contaminant hydrology*, 66(3-4):161-78.

Li, L., Benson, C. H., Lawson, E.M., 2005. Impact of Mineral Fouling on Hydraulic Behavior of Permeable Reactive Barriers. *Ground Water*, 43(4):582-596.

Liang, L.Y., Moline, G.R., Kamolpornwijit, W., and West, O.R., 2005. Influence of Hydrogeochemical Processes on Zero-valent Iron Reactive Barrier Performance : A Field Investigation. *Journal of Contaminant Hydrology*, 78: 291-312.

Mackenzie, P.D., Horney, D.P., Sivavec, T.M., 1999. Mineral Precipitation and Porosity Losses in Granular Iron Columns. *Journal of Hazardous Materials*, 68(1-2):1-17.

Mayer,K.U., Blowes, D.W., Frind, E.Q., 2001. Reactive Transport Modeling of An in Situ Reactive Barrier for the Treatment of Hexavalent Chromium and Trichloroethylene in Groundwater. Water Resour. Res. 37(12): 3091-3103.

Parkhurst, D.L., Appelo, C. A. J.,1999. User's Guide to PHREEQC (version 2)-A Computer Program for Speciation, Batch-reaction, One-dimensional Transport, and Inverse Geochemical Calculations. U.S. Geological Survey Water-Resources Investigations Report.

Prommer, H., Aziz, L. H., Bolaño,N., 2008. Modelling of Geochemical and Isotopic Changes in A Column Experiment for Degradation of TCE by Zero-valent Iron. *Journal of Contaminant Hydrology*, 97(1-2): 13–26.

Robertson, W. D., Cherry, J.A., 1995. In Situ Denitrification of Septic-System Nitrate Using Reactive Porous Media Barriers: Field Trials [J]. *Ground Water*, 33(1): 99-111.

Robertson, W.D., Ptacek, C.J., Brown, S.J., 2007. Geochemical and Hydrogeological Impacts of A Wood Particle Barrier Treating Nitrate and Perchlorate in Ground Water. *Ground Water*, 27(2):85-95.

Robertson, W.D., Vogan, J.L., Lombardo, P.S., 2008. Nitrate Removal Rates in a 15-year-old Permeable Reactive Barrier Treating Septic System Nitrate. *Ground Water Monitoring and Remediation*, *28*(3):65–72.

Robertson, W.D., Blowes, D.W., Ptacek, C.J., et al., 2000. Long-Term Performance of in Situ Reactive Barriers for Nitrate Remediation. *Ground Water*, 38(5): 689-695.

Rodríguez-Maroto, J.M., García-Herruzo, F., García-Rubio, A., et al., 2009. Kinetics of the Chemical Reduction of Nitrate by Zero-Valent Iron. *Chemosphere,* 74(6):804-809.

RTDF. 2001. Permeable Reactive Barrier Installation Pro-

files.
http://www.rtdf.org/public/permbarr/prbsumms/default.cfm.

Schipper, L., Vojvodić-Vuković, M., 1998. Nitrate Removal from Groundwater Using a Denitrification Wall Amended with Sawdust : Field Trial. *Journal of Environmental Quality*, 27(3):664-668.

Till, B. A., Weathers, L. J., Alvarez, P. J., 1998. Fe(0)-Supported Autotrophic Denitrification. Environ. Sci. Technol, 32(5):634-639.

Wilkin, R.T., Puls, R.W., Sewelll, et al., 2002. Long-Term Performance of Permeable Reactive Barriers Using Zero-Valent Iron-Geochemical and Microbiological Effects. *Ground Water*, 41(4):493-503.

Thiruvenkatachari, R., Vigneswaran, S., Naidu, R., 2008. Permeable Reactive Barrier for Groundwater Remediation. *Environmental Protection*, 14(2):145-156.

Vogan, J.L., Focht, R.M., Clark, D.K., et al., 1999. Performance Evaluation of a Permeable Reactive Barrier for Remediation of Dissolved Chlorinated Solvents in Groundwater. *Journal of Hazardous Materials*, 68(1/2): 97-108.

Zhang, J., Hao, Z., Zhang, Z., et al., 2010. Kinetics of Nitrate Reductive Denitrification by Nanoscale Zero-Valent Iron. *Process Safety and Environmental Protection*, 88(6): 439-445.

Zhang, Z., Hao, Z., Yang,Y., 2010. Reductive Denitrification Kinetics of Nitrite by Zero-Valent Iron. *Desalination*, 257(1/3):158-162.

Zhang, Y., Gillham, R.W., 2005. Effects of Gas Generation and Precipitates on Performance of Fe^0 PRBs. *Ground Water*, 43(1): 113-121.

Zheng, C., Wang, P. P., 1999. MT3DMS: A Modular Three-Dimensional Multispecies Transport Model for Simulation of Advection , Dispersion , and Chemical Reactions of Contaminants in Groundwater Systems; Documentation and User's Guide. Contract Report SERDP-99-1, U.S. Vicksburg, Mississippi: Army Engineer Research and Development Center.